

RESEARCH LETTER

Undifferentiated
Induced Pluripotent
Stem Cells as
a Genetic Model
for Nonalcoholic
Fatty Liver
Disease

Q5 Patient-derived induced pluripotent stem cells (iPSCs) have been transformational in biomedical research for their ability to differentiate into any cell type while retaining the genetic information of the donor individual, for example iPSC-derived hepatocyte-like cells (iPSC-Heps) for studies of nonalcoholic fatty liver disease (NAFLD).¹ However, differentiation protocols are time-intensive, use costly reagents, require highly specialized training, and can result in

heterogeneous cultures that are limited in number.² Thus, iPSC-Heps are poorly suited for studies of genetic variation that require scalability and reproducibility. In contrast, iPSCs exhibit self-renewal, can be cryopreserved, have standardized and robust protocols available for their generation and culturing, and are substantially less expensive to produce. We tested whether iPSCs in their undifferentiated state may be an informative to model genetic factors underlying NAFLD. NAFLD is initiated by hepatic steatosis, often attributed to excess synthesis, retention, or uptake of fatty acids by the liver, where they are stored as triglycerides within lipid droplets. As nearly all cells can take up fatty acids, synthesize triglycerides, and create lipid droplets,³ we sought to determine whether iPSCs could model fatty acid induced lipid accumulation.

Authenticated iPSCs (Supplementary Table 1) were

previously described.⁴ We confirmed that a representative iPSC accumulates intracellular lipids in response to 24-hour oleate challenge in a dose dependent manner, with lipids detected by 2 neutral lipid stains (Nile Red and LipidTox Red) and through Simulated Raman Spectroscopy, a highly specific detection method for unlabeled triglycerides⁵ (Figure 1, A–B). To improve quantitation accuracy, we developed a flow cytometry-based assay (Figure 1, C), resulting in highly reproducible measures (Figure 1, D), which confirmed that oleate treatment increased intracellular lipids in cell lines from 30 donors (2.0 ± 0.11 fold mean \pm standard error; $P = 4.0 \times 10^{-10}$) (Figure 1, E; Supplementary Table 2).

We next compared the degree of oleate-induced lipid accumulation in iPSCs from 8 donors both in their undifferentiated state and after differentiation into iPSC-Heps through a 23-day protocol as we previously

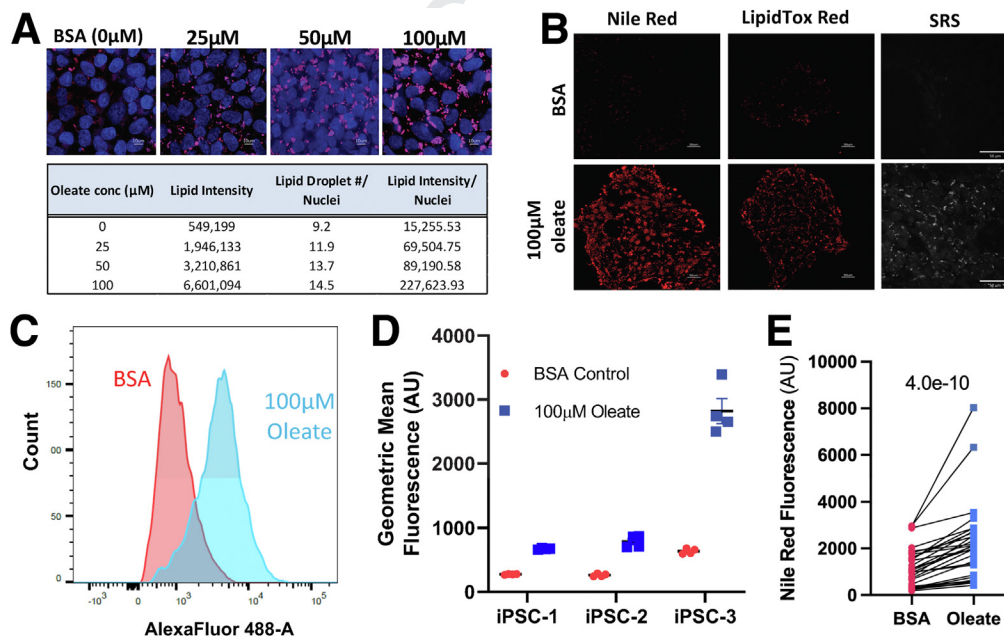


Figure 1. iPSCs accumulate intracellular lipids when challenged with oleate. (A) Images taken at 100 \times magnification of an iPSC line challenged for 24 hours with (0–100 μ M) sodium oleate conjugated to bovine serum albumin (BSA). Cells were stained with 10 μ g/mL of Nile Red (pink) to visualize lipid droplets and Hoescht (blue) to stain nuclei. 10- μ m size bars shown. (B) Oleate- vs BSA-treated iPSCs were stained with Nile Red or LipidTox Red and visualized via fluorescence microscopy. A separate aliquot of cells was left unstained and subjected to SRS microscopy, in which unstained triglycerides are visualized as white areas. 50- μ m size bars shown. (C) Representative histogram of Nile Red fluorescence values of BSA- and 100 μ M oleate-treated iPSCs. Cells were stained with Nile Red prior to quantitation by flow cytometry. (D) Biological replicate measures of intracellular lipid levels in iPSCs from 3 donors (n = 4). (E) Geometric means of the Nile Red fluorescence values indicative of intracellular lipids in 30 iPSC lines treated with BSA and 100 μ M oleate.

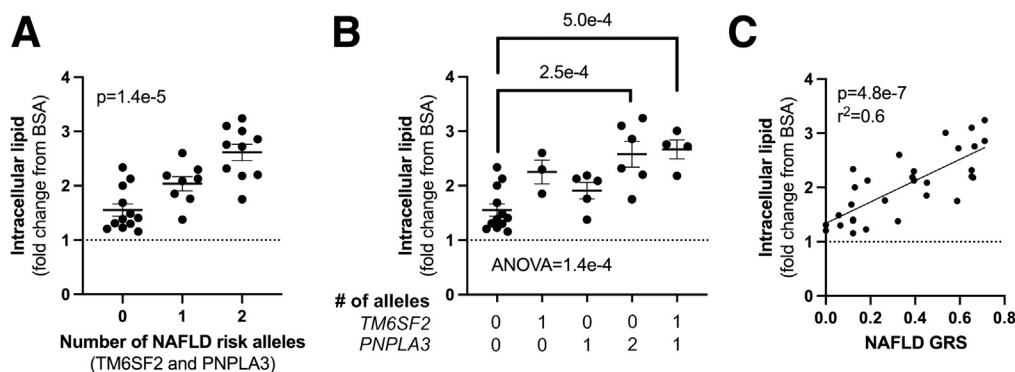


Figure 2. The magnitude of oleate-induced intracellular lipid accumulation in undifferentiated iPSCs is correlated with NAFLD genetic risk. Oleate-induced intracellular lipid accumulation was quantified in iPSCs from 30 donors as described in Figure 1, and the fold change in lipid accumulation was plotted separated by the number of NAFLD risk alleles for *TM6SF2* and/or *PNPLA3* together (A) or separately (B). Linear regression (panel A) and analysis of variance with posthoc multiple comparisons against the 0 allele carrier group was performed with adjusted *P*-values (panel B) are shown. (C) Correlation of intracellular lipid accumulation with 4-SNP NAFLD genetic risk score.

described.⁶ iPSC-Heps were authenticated by expression of hepatocyte markers and secretion of albumin into the culture media (Supplemental Figure 1, A–B). There were no differences in the levels of intracellular lipids in the isogenic iPSCs and iPSC-Heps, either with values expressed as absolute levels or the magnitude of change between oleate vs BSA treated cells (Supplemental Figure 1, C–E).

Variants in *TM6SF2* (rs58542926), *PNPLA3* (rs738409), *GCKR* (rs1260326), and *MBOAT7* (rs641738) are all associated with NAFLD in multiple independent cohorts, and have published effect sizes for their association with hepatic fat.⁷ All 4 genes had detectable expression in undifferentiated iPSCs, unlike lymphoblastoid cell lines, another patient-derived cell line (Supplemental Figure 2). Importantly, iPSCs carrying increasing numbers of rs58542926 and rs738409 NAFLD risk alleles had greater intracellular lipid accumulation with an additive relationship observed ($P = 1.4 \times 10^{-5}$) (Figure 2, A). The magnitude of this effect was nearly identical between the 2 risk alleles, consistent with their reported effect sizes⁷ (Figure 2, B). Moreover, we found a significant positive correlation ($r^2 = 0.60$; $P = 4.8 \times 10^{-7}$) between oleate-induced intracellular lipid accumulation and a weighted genetic risk score based on the reported associations of *TM6SF2* rs58542926, *PNPLA3* rs738409, *GCKR* rs1260326,

and *MBOAT7* rs641738 alleles with hepatic fat⁷ (Figure 2, C).

Here, we show that patient-derived iPSCs in their undifferentiated state can be used to model genetic factors that influence individual-level variation in fatty-acid induced lipid accumulation, critical in NAFLD pathobiology. Compared with iPSC-Heps or liver organoids, iPSCs are significantly more scalable, enabling their use for genetic discovery. This could support future use of iPSCs for identifying high-risk individuals, testing variation in response to treatment, and informing the development of precision medicine guidelines for NAFLD prevention and management. Our results also raise the possibility of using iPSCs for investigating genetic influences on other diseases characterized by excess lipid storage. Notably, both the *TM6SF2* rs58542926 and *PNPLA3* rs738409 risk variants are thought to cause lipid accumulation in hepatocytes by impairing intracellular lipid transport and reducing triglyceride secretion in APOB-containing lipoprotein particles,^{8,9} processes that has not been identified in iPSCs. Additional study is needed to assess the mechanisms underlying these relationships and determine the extent to which NAFLD relevant pathways can be modeled in the iPSC. Lastly, these findings challenge the current paradigm of iPSC use, which assumes that cells must be

differentiated to be informative, highlighting the potential utility of undifferentiated patient-derived iPSCs as a cellular model of individual level disease risk.

ANTONIO MUÑOZ
ELIZABETH THEUSCH
YU-LIN KUANG
GILBERT NALULA
Department of Pediatrics
University of California San Francisco
San Francisco, CA

CAITLIN PEASLEE
Department of Pathology
University of California San Francisco
San Francisco, CA

GABRIEL DORLHIAC
Biophysics Graduate Group
University of California Berkeley
Berkeley, CA

MARKITA P. LANDRY
Department of Chemical and Biomolecular Engineering
University of California Berkeley
Berkeley, CA
Chan Zuckerberg Biohub
San Francisco, CA

AARON STREETS
Biophysics Graduate Group
University of California Berkeley
Berkeley, CA
Chan Zuckerberg Biohub
San Francisco, CA

235 Department of Bioengineering
236 University of California Berkeley
237 Berkeley, CA
238
239 **RONALD M. KRAUSS**
240 Department of Pediatrics
241 University of California San Francisco
242 San Francisco, CA and
243 Department of Medicine
244 University of California San Francisco
245 San Francisco, CA

246 **CARLOS IRIBARREN**
247 Kaiser Permanente Division of
248 Research
249 Oakland, CA

250 **ARAS N. MATTIS**
251 Department of Pathology
252 University of California San Francisco
253 San Francisco, CA and
254 Liver Center
255 University of California San Francisco
256 San Francisco, CA

257 **MARISA W. MEDINA**
258 Department of Pediatrics
259 University of California San Francisco
260 San Francisco, CA

261 Correspondence

262 Address correspondence to: Dr Marisa Medina,
263 Department of Pediatrics, University of California San
264 Francisco, San Francisco, CA 94143. e-mail: [marisa.
265 medina@ucsf.edu](mailto:marisa.medina@ucsf.edu)

266 References

- 267
268
269 1. Boeckmans J, et al. *Pharmacol*
270 *Res* 2018;257–267.
271 2. Godoy P, et al. *Arch Toxicol*
272 2013;1315–1530.

3. Bosch M, et al. *Science* 2020;
370:eaay8085.
4. Kuang YL, et al. *Stem Cell Res*
2019;101434.
5. Cao C, et al. *Anal Chem* 2016;
4931–4839.
6. Peaslee C, et al. *Hepatology*
2021;2102–2177.
7. Dongiovanni P, et al. *J Intern*
Med 2018;356–370.
8. Diraison F, et al. *Diabetes Metab*
2003;478–485.
9. Donnelly KL, et al. *J Clin Invest*
2005;1343–1351.

Abbreviations used in this paper: iPSCs, induced pluripotent stem cells; iPSC-Hep, iPSC-derived hepatocyte-like cells; NAFLD, nonalcoholic fatty liver disease.

© 2022 The Authors. Published by Elsevier Inc. on behalf of the AGA Institute. This is an open access article under the CC BY-NC-ND license (<http://creativecommons.org/licenses/by-nc-nd/4.0/>).
2352-345X
<https://doi.org/10.1016/j.jcmgh.2022.07.009>

Received June 23, 2022. Accepted July 12, 2022.

Acknowledgment

The authors thank all of the POST participants without whom this study would not be possible, as well as Meng Lui and Gabriela Sanchez for their assistance with recruitment. Kristin Stevens assisted with RNAseq library preparation, and some iPSCs were generated by the University of Florida iPSC Core. Aaron Streets and Markita P. Landry are Chan Zuckerberg Biohub Investigators. Aaron Streets is a Pew Biomedical Scholar.

CRedit Authorship Contributions

Antonio Munoz-Howell, MSc (Data curation: Lead; Formal analysis: Lead; Investigation: Lead; Methodology: Lead; Validation: Lead; Visualization: Lead; Writing – original draft: Lead; Writing – review & editing: Lead)
Elizabeth Theusch, PhD (Investigation: Supporting; Writing – review & editing: Equal)
Yu-Lin Kuang, PhD (Investigation: Supporting; Writing – review & editing: Supporting)
Gilbert Nalula, BS (Investigation: Supporting; Writing – review & editing: Supporting)
Caitlin Peaslee, BS (Investigation: Supporting; Writing – review & editing: Supporting)
Gabriel Dorliac, PhD (Investigation: Supporting; Visualization: Supporting; Writing – review & editing: Supporting)
Markita P. Landry, PhD (Visualization: Supporting; Writing – review & editing: Supporting)
Aaron Streets, PhD (Visualization: Supporting; Writing – review & editing: Supporting)
Ronald Krauss, PhD (Funding acquisition: Equal; Supervision: Supporting; Writing – review & editing: Supporting)
Carlos Iribarren, PhD (Funding acquisition: Equal; Writing – review & editing: Supporting)
Aras N. Mattis, PhD (Conceptualization: Equal; Funding acquisition: Equal; Investigation: Supporting; Methodology: Supporting; Supervision: Supporting; Writing – review & editing: Supporting)
Marisa Medina, PhD (Conceptualization: Lead; Data curation: Supporting; Funding acquisition: Lead; Supervision: Lead; Writing – original draft: Equal; Writing – review & editing: Equal)

Conflicts of interest

This author discloses the following: Aras N. Mattis is a consultant for Hepatx, Ambys Medicines, and BioMarin. The remaining authors disclose no conflicts.

Funding

This work was supported by the National Institutes of Health P50 GM115318 (Marisa W. Medina, Ronald M. Krauss), R01DK127718 (Marisa W. Medina, Aras N. Mattis), P30 DK026743 (Aras N. Mattis), the National Science Foundation 1845623 (Aaron Streets), and the Program for Breakthrough Biomedical Research, which is partially funded by the Sandler Foundation (Marisa W. Medina, Aras N. Mattis). The funding agencies had no role in the study design, analysis, or interpretation of data.

Supplementary Materials and Methods

Post Induced Pluripotent Stem Cell (iPSC) Donor Demographics

Cell line donors were genotyped on Illumina Infinium OmniExpressExome bead chips. Thirty-five iPSC lines were selected for this study based on their sex, ancestry, and genetic information (Supplementary Table 1). Because most of the nonalcoholic fatty liver disease (NAFLD) genetic studies have been performed in individuals of European ancestry, we used cell lines from donors of European descent so the effect sizes and genetic risk score would be most accurate.

iPSC and iPSC-derived Hepatocyte-like (iPSC-Hep) Cell Culture

iPSCs were cultured in mTESR1 media at 37 °C at 5% CO₂. iPSCs were passaged using accutase (Stemcell Technologies, Cat. # 07920) and media supplemented with Y-27632 2HCl inhibitor (Selleckchem, Cat. # S1049). iPSC-Heps were cultured at 37 °C and 5% CO₂ in Lonza Hepatocyte Culture Medium (HCM; Cat. # CC-3198). iPSCs were differentiated into hepatoblasts as previously published.¹ Expression of hepatocyte-specific markers albumin and hepatic nuclear factor 4 alpha (HNF4A) were confirmed by fluorescence-activated cell sorting at a threshold of >90% dual-positive cells.

Intracellular Lipid Accumulation

iPSCs and iPSC-Heps were grown to 70% to 75% confluency in 6-well plates. Cell lines were challenged with HCM containing 0 to 100 μM oleate conjugated to fatty acid-free (FAF) bovine serum albumin (BSA), and all BSA-containing supplements were removed. A volume of FAF-BSA equivalent to the oleate condition was used as a negative control. After 24 hours, cells were fixed with 10% paraformaldehyde.

Flow Cytometry for Quantification of Intracellular Lipids

Cells were stained with Nile Red (Sigma, Cat. # 72485) diluted to 100 μg/mL in Dulbecco's phosphate-buffered saline for 30 minutes, and fluorescence was quantified using the BD LSRFortessa. Data was analyzed using FloJo v10.7.1. Oleate-induced increases in cellular lipids were quantified as the fold change of the oleate-treated/BSA-treated cells. Two outliers were identified using the ROUT test. Because they were from the same batch of samples, all 5 samples in the batch were excluded from the analyses, resulting in a sample size of n = 30. Paired Student *t* tests were used to identify statistically significant differences between BSA- and oleate-treated cells. Linear regression was used to evaluate the correlation between variation in the magnitude of oleate-induced increase in intracellular lipid accumulation and the number of *TM6SF2* rs58542926 and/or *PNPLA3* rs738409 risk alleles. All statistical analyses were performed using JMP Pro 16.0.0 and GraphPad Prism version 9.1.0.

Calculation of a Weighted NAFLD Genetic Risk Score

A 4 single nucleotide polymorphism (SNP)-weighted genetic risk score (GRS) was calculated for each iPSC line using the following variants: *PNPLA3* rs738409, *TM6SF2* rs58542926, *GCKR* rs1260326, and *MBOAT7* rs641738 using previously estimated effect sizes for their relationships with hepatic fat.² The DHS coefficients used were 0.2653 for each rs738409 G allele, 0.2711 for each rs58542926 T allele, 0.0649 for each rs1260326 T allele, and 0.0575 for each rs641738 T allele. The GRS was calculated as the sum of the product of the weights for each SNP and the numbers of each risk allele present.

Fluorescence Microscopy

Cells were stained with Nile Red (100 μg/mL) and Hoescht 33342 (5

μg/mL) for 30 minutes (ThermoFisher, Cat. # H3570). Images were captured on a Keyence BZX-700 microscope at 100× and 20× magnification using phase contrast and widefield fluorescence microscopy. Fiji was used to quantify both nuclei and lipid droplet counts as well as the integrated intensity of lipid droplets in 100× images.

Stimulated Raman Spectroscopy (SRS) Microscopy

The dual output of a commercial oscillator/optical parametric oscillator (Insight DS+, Spectra-Physics) was used for SRS imaging. The output of the optical parametric oscillator was set to 802 nm corresponding to a wavenumber of ~2850 cm⁻¹ with the fundamental at 1040 nm used as the Stokes field. The fundamental was amplitude modulated at 10.28 MHz using a resonant EOM (EO-AM-R-C2, Thorlabs) and a Glan-laser polarizer (Thorlabs). The 802 and 1040 nm beams were combined on a 1000 nm short-pass dichroic mirror (Thorlabs) and fed into a commercial inverted scanning microscope (Olympus IX83-FV1200). Temporal coincidence of the pulses was controlled using a variable delay stage placed on the 802 nm arm (FCL200, Newport). A 60× water-immersion objective (1.2 NA) was used for imaging (UPLSAPO60XWIR, Olympus), with a 1.4 NA oil-immersion condenser (CSC1003, Thorlabs) used to collect the light sent to the detector. The Stokes beam was blocked using a 1000 nm shortpass filter (Thorlabs), and the 802 nm pump was detected on a photodiode reverse biased at 61.425 V. The output of the photodiode was demodulated by a lock-in amplifier (H2FLI, Zurich Instruments) for image formation. All images were acquired at 512 × 512 pixels per field of view, using a pixel dwell time of 10 μs, and a lock-in time constant of 3 μs. The average power of both the 802 and 1040 nm lines was 10 mW. Intracellular lipid content was measured as the integrated SRS signal at 2850 cm⁻¹,

471 which primarily corresponds to CH₂
 472 stretching in lipid molecules. To
 473 calculate average cellular lipid content,
 474 the images were pseudo-flatfield cor-
 475 rected using a Gaussian convolved
 476 version of the image as the flatfield
 477 (with radius equal to 150 pixels). A
 478 thresholded cellular image for each
 479 field of view was then produced by
 480 first lowpass filtering the image, and
 481 then performing an adaptive local his-
 482 togram equalization (with radius of 15
 483 pixels).

485 *RNA Sequencing Analysis*

486 Isolated RNA was prepared into
 487 polyA-selected, strand-specific
 488 sequencing libraries for 100 bp paired-

489 end sequencing at the Northwest Ge-
 490 nomics Center. Gene expression levels
 491 in iPSCs were compared with previ-
 492 ously generated RNAseq data,
 493 including 426 lymphoblastoid cell
 494 lines,^{3,4} primary human hepatocytes
 495 from 4 donors (Supplementary Ta-
 496 ble 3), and 10 biological replicates
 497 HepG2. GTEx V8 liver TPM expression
 498 levels were downloaded via the GTEx
 499 portal for comparison. Sequence tran-
 500 script counts per million (TPM) were
 501 calculated by dividing the number of
 502 sequence fragments aligning to the
 503 gene by the gene length in kilobases
 504 (FPK). The sum of the FPK for each
 505 gene across all samples was then
 506 divided by one million to create a

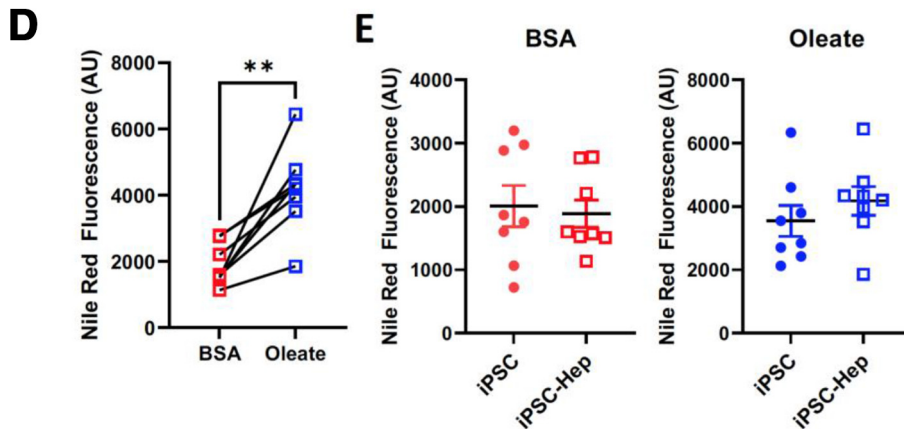
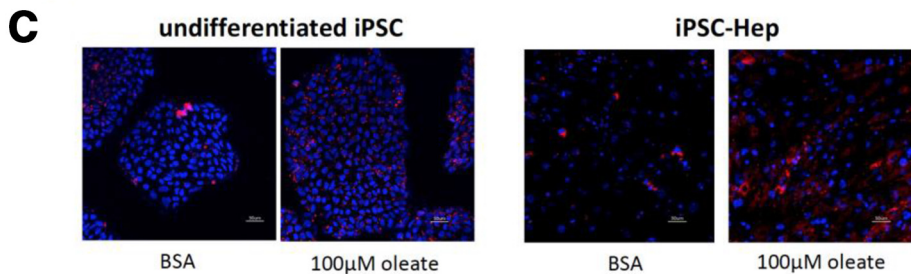
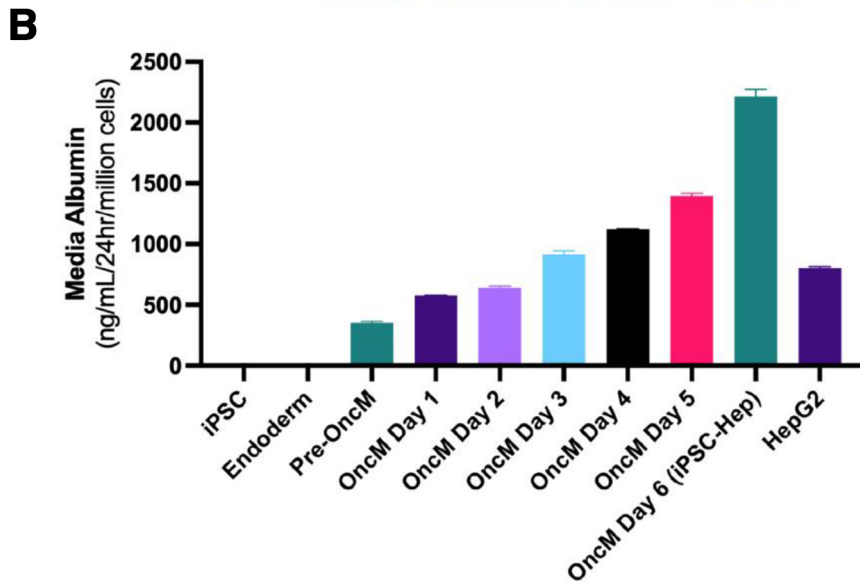
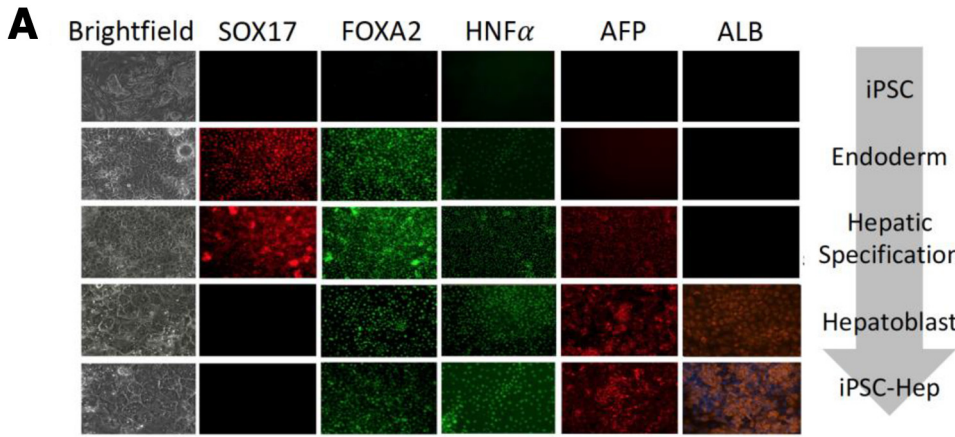
507 scaling factor (FPK/million). The FPK
 508 for each sample and gene were then
 509 divided by the scaling factor for that
 510 gene to create the final TPM value.
 511 These values were graphed using
 512 Graphpad prism 9.1.0 and shown as
 513 Log₁₀ TPM.

514 **References**

- 515 1. Peaslee C, et al. *Hepatology*
 516 2021;74:2102–2117.
- 517 2. Dongiovanni P, et al. *Biomed Res*
 518 *Int* 2015;2015:460190.
- 519 3. Theusch E, et al. *Pharmacoge-*
 520 *nomics J* 2017;17:222–229.
- 521 4. Theusch E, et al. *BMC Genomics*
 522 2020;21:555.

589
590
591
592
593
594
595
596
597
598
599
600
601
602
603
604
605
606
607
608
609
610
611
612
613
614
615
616
617
618
619
620
621
622
623
624
625
626
627
628
629
630
631
632
633
634
635
636
637
638
639
640
641
642
643
644
645
646
647

648
649
650
651
652
653
654
655
656
657
658
659
660
661
662
663
664
665
666
667
668
669
670
671
672
673
674
675
676
677
678
679
680
681
682
683
684
685
686
687
688
689
690
691
692
693
694
695
696
697
698
699
700
701
702
703
704
705
706

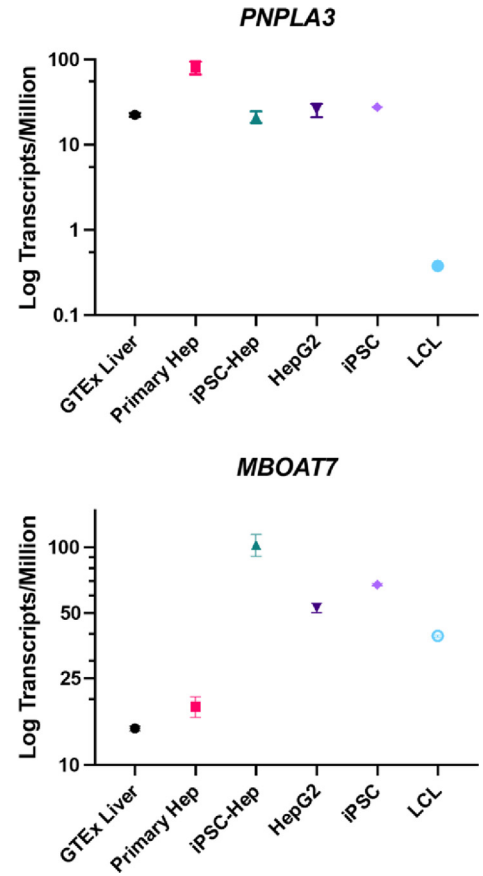
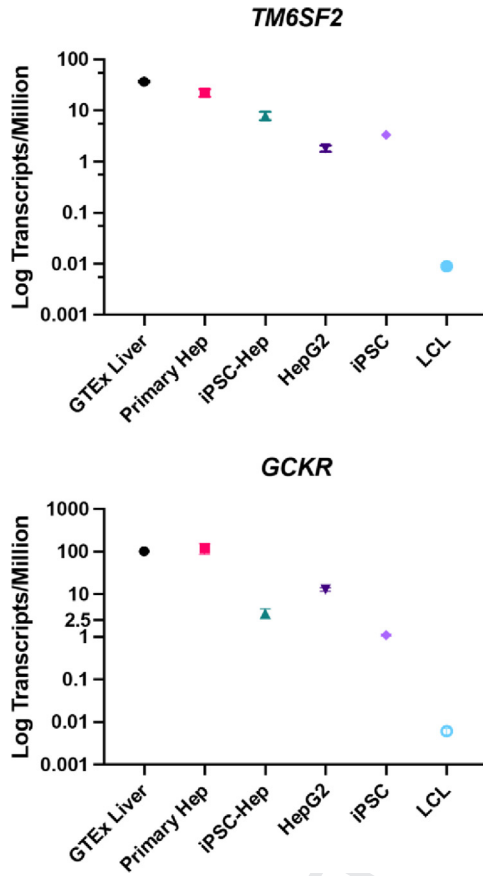


Supplementary Figure 1. Authentication of iPSC-Heps and comparison with iPSCs. (A) Brightfield and fluorescence microscopy of iPSCs during differentiation into iPSC-Heps with immunohistochemical evaluation of endoderm (SOX17, FOX2A), and hepatocyte markers (HNFα, alpha fetal protein [AFP], albumin [ALB]) during various stages of differentiation. (B) Albumin in the culture media of iPSCs during differentiation into iHeps and compared with the human hepatoma cell line HepG2. Oncostatin M day 1 to day 5 represent the stage of hepatoblast formation and differentiation into iPSC-Heps at day 6 after addition of oncostatin M (or day 23 after initiating the differentiation protocol). Values shown are mean ± standard error of the mean. (C) Oleate-induced intracellular lipids were imaged at 20× magnification in undifferentiated iPSCs and iPSC-Heps as described in Figure 1. 50-µm size bars shown. (D) iPSC-Heps were treated with BSA or 100 µM oleate (n = 8), and Nile Red fluorescence was quantified by fluorescence-activated cell sorting. **P = .0018, paired t test. (E) Intracellular lipid accumulation was quantified in iPSCs from 8 unique donors before and after differentiation into iPSC-Heps, and after treatment with 100 µM oleate or bovine serum albumen control.

707
708
709
710
711
712
713
714
715
716
717
718
719
720
721
722
723
724
725
726
727
728
729
730
731
732
733
734
735
736
737
738
739
740
741
742
743
744
745
746
747
748
749
750
751
752
753
754
755
756
757
758
759
760
761
762
763
764
765

web 4C/FPO

Supplementary Figure 2. Undifferentiated iPSCs express genes identified by NAFLD genetic association analyses. PolyA-selected whole transcriptome sequencing was performed in GTEx liver (n = 226), primary human hepatocytes (n = 4), human iPSCs (n = 48), the human hepatoma HepG2 cell line (n = 10), and human lymphoblastoid cell lines (n = 426), and *TM6SF2*, *PNPLA3*, *GCKR*, and *MBOAT7* transcript levels were quantified as transcripts per million. The y-axis is scaled as Log₁₀. Primary hepatocytes were obtained from 3 female and 1 male donor between the ages of 49 and 75 years with body mass index ranging from 22.5 to 24.3 kg/m².



766
767
768
769
770
771
772
773
774
775
776
777
778
779
780
781
782
783
784
785
786
787
788
789
790
791
792
793
794
795
796
797
798
799
800
801
802
803
804
805
806
807
808
809
810
811
812
813
814
815
816
817
818
819
820
821
822
823
824

Supplementary Table 1. Demographic and Genetic Characteristics of iPSC Donors

iPSC line	Sex	Ancestry	<i>PNPLA3</i> rs738409 # of G alleles	<i>TM6SF2</i> rs58542926 # of T alleles	4 SNP-weighted GRS
1	F	European	0	1	0.451
2	M	European	0	1	0.329
3	F	European	0	1	0.394
4	M	European	0	0	0.058
5	M	European	0	0	0.122
6	M	European	0	0	0.187
7	F	European	0	0	0.122
8	F	European	0	0	0.065
9	F	European	0	0	0.000
10	F	European	0	0	0.122
11	F	European	0	0	0.180
12	M	European	0	0	0.115
13	F	European	0	0	0.000
14	F	European	0	0	0.122
15	M	European	0	0	0.130
16	F	European	1	0	0.395
17	F	European	1	0	0.388
18	F	European	1	0	0.323
19	M	European	1	0	0.453
20	M	European	1	0	0.265
21	F	European	1	1	0.659
22	M	European	1	1	0.594
23	M	European	1	1	0.666
24	F	European	1	1	0.536
25	F	European	2	0	0.653
26	M	European	2	0	0.711
27	F	European	2	0	0.653
28	M	European	2	0	0.653
29	M	European	2	0	0.711
30	M	European	2	0	0.588

Note: Informed consent was obtained from all study subjects for the creation of induced pluripotent stem cells, and studies were performed with institutional review board approval of both Kaiser Permanente Northern California and the University of California San Francisco Benioff Children's Hospitals. Donor individuals were genotyped using Illumina Infinium OmniExpressExome bead chips. A 4 SNP-weighted GRS was calculated for each iPSC line using the following variants: *PNPLA3* rs738409, *TM6SF2* rs58542926, *GCKR* rs1260326, and *MBOAT7* rs641738.

F, Female; GRS, genetic risk score; iPSCs, induced pluripotent stem cells; M, male; SNP, single nucleotide polymorphism.

Supplementary Table 2. Flow Cytometry Values of iPSCs Post Oleate Challenge and Nile Red Staining

iPSC line	BSA geometric mean	100 μ M oleate geometric mean
1	1556	2880
2	661	1718
3	185	425
4	388	579
5	241	563
6	245	521
7	2038	2874
8	1487	1940
9	981	1285
10	1887	2185
11	2881	3549
12	1601	2698
13	1754	2123
14	974	1356
15	1059	2118
16	2971	6331
17	1502	3293
18	1814	2510
19	1121	2345
20	1141	2004
21	1266	2758
22	2952	8028
23	717	1982
24	255	767
25	965	2120
26	790	2559
27	274	637
28	469	1456
29	302	864
30	349	611

BSA, Bovine serum albumin; iPSCs, induced pluripotent stem cells.

943
944
945
946
947
948
949
950
951
952
953
954
955
956
957
958
959
960
961
962
963
964
965
966
967
968
969
970
971
972
973
974
975
976
977
978
979
980
981
982
983
984
985
986
987
988
989
990
991
992
993
994
995
996
997

998
999
1000
1001
1002
1003
1004
1005
1006
1007
1008
1009
1010
1011
1012
1013
1014
1015
1016
1017
1018
1019
1020
1021
1022
1023
1024
1025
1026
1027
1028
1029
1030
1031
1032
1033
1034
1035
1036
1037
1038
1039
1040
1041
1042
1043
1044
1045
1046
1047
1048
1049
1050
1051
1052